Creating von Laue patterns in crystal scattering with partially coherent sources

Yangyundou Wang
School of Marine Science and Technology/School of Electronics and Information, Northwestern Polytechnical University, 710072 Xian, China

David Kuebel
St. John Fisher College, Rochester, New York 14618, USA
and Department of Physics and Astronomy, University of Rochester, Rochester, New York 14627, USA

Taco D. Visser
School of Marine Science and Technology/School of Electronics and Information, Northwestern Polytechnical University, 710072 Xian, China;
Department of Physics and Astronomy, University of Rochester, Rochester, New York 14627, USA;
Department of Physics and Astronomy, Vrije Universiteit, 1081 HV Amsterdam, The Netherlands;
and Department of Electrical Engineering, Delft University of Technology, 2620 CD Delft, The Netherlands

Emil Wolf
Department of Physics and Astronomy, University of Rochester, Rochester, New York 14627, USA
and Institute of Optics, University of Rochester, Rochester, New York 14627, USA
(Received 7 June 2016; published 9 September 2016)

When spatially coherent radiation is diffracted by a crystalline object, the field is scattered in specific directions, giving rise to so-called von Laue patterns. We examine the role of spatial coherence in this process. Using the first-order Born approximation, a general analytic expression for the far-zone spectral density of the scattered field is obtained. This equation relates the coherence properties of the source to the angular distribution of the scattered intensity. We apply this result to two types of sources. Quasihomogeneous Gaussian Schell-model sources are found to produce von Laue spots whose size is governed by the effective source width. Delta-correlated ring sources produce von Laue rings and ellipses instead of point-like spots. In forward scattering, polychromatic ellipses are created, whereas in backscattering striking, overlapping ring patterns are formed. We show that both the directionality and the wavelength-selectivity of the scattering process can be controlled by the state of coherence of the illuminating source.

DOI: 10.1103/PhysRevA.94.033812

I. INTRODUCTION

The diffraction of radiation by a three-dimensional, periodic potential, i.e., from a crystalline object, is a subject whose origins were developed a century ago by von Laue, Friedrich, Knipping, and the Bragg father-son team [1]. Specifically, in the von Laue method, broad spectrum radiation, which is assumed to be spatially coherent, is diffracted by a monocrystal with a fixed orientation [2, Ch. 6]. The resulting diffraction peaks are separated both spatially and spectrally. The location of these von Laue spots is determined by the crystal's structure [3, Sec. 13.1.3]. Here we report how the state of spatial coherence of the incident field can drastically affect their size, shape, and spectral composition.

The influence of the state of coherence of the incident field on the scattering process has been investigated in several publications; see, for example, Refs. [4–12]. These studies were all concerned with either spherical particles, cylinders, or planar scatterers. In contrast, scattering of partially coherent fields by a medium with a periodic potential has remained largely unexplored. Notable exceptions are a study by Dušek [13], who described dispersion effects in crystal scattering with completely incoherent radiation, and a paper by Hoenders and Bertolotti [14], in which the van Cittert-Zernike theorem was generalized to two-dimensional periodic media. Recently, a more general approach to this problem was suggested in Ref. [15], although there the analysis was limited to one-dimensional scatterers.

In the present paper we study the scattering properties of media with a periodic, three-dimensional scattering potential. We begin by analyzing the scattering of an incident field, generated by a source with an arbitrary state of spatial coherence, by a general mono-crystalline structure of identical point scatterers. We then examine the special case of large, three-dimensional arrays of scatterers whose unit cells are rectangular parallelepipeds. Such cells form *orthorhombic crystals* [16]. The incident field is taken to be generated by a planar, partially coherent source that is located far away from the crystal. The use of the first-order Born approximation allows us to derive an analytic expression for the spectral density of the far-zone scattered field in terms of a correlation function of the source, namely its *cross-spectral density* [17, Sec. 4.3.2]. We then apply this result to two types of sources. Gaussian Schell-model (GSM) sources [17, Sec. 5.2.2] generate an incident field that is Gaussian correlated. Such fields are found to give rise to larger von Laue diffraction spots than those produced by their spatially fully coherent counterparts. When the GSM source is also quasihomogeneous [17, Sec. 5.2.2], the spot size is directly related to the source width. For the case of a δ-correlated annular source, the incident field is J_0-correlated. This can produce multicolored, elliptical von Laue patterns in the forward direction and an overlapping, multiple ring

pattern in the backward direction. Our results show that both the directionality and the wavelength-selectivity of the scattering process can be controlled by altering the state of coherence of the illuminating source or the distance between the annular source and the crystal.

II. SCATTERING FROM CRYSTALLINE STRUCTURES

The incident field at position $\mathbf{r}$ and at frequency $\omega, U^{(\mathrm{in})}(\mathbf{r},\omega)$, is taken to be partially coherent. In the space-frequency domain formulation of coherence theory, its correlation properties are characterized by the *cross-spectral density function* [18],

$$W^{(\mathrm{in})}(\mathbf{r}_1,\mathbf{r}_2,\omega) = \langle U^{(\mathrm{in})*}(\mathbf{r}_1,\omega)U^{(\mathrm{in})}(\mathbf{r}_2,\omega)\rangle, \tag{1}$$

where the angular brackets denote an average taken over an ensemble of realizations of the field, and the asterisk indicates complex conjugation. The normalized version of this correlation function is the *spectral degree of coherence*,

$$\mu^{(\mathrm{in})}(\mathbf{r}_1,\mathbf{r}_2,\omega) = \frac{\langle U^{(\mathrm{in})*}(\mathbf{r}_1,\omega)U^{(\mathrm{in})}(\mathbf{r}_2,\omega)\rangle}{[S^{(\mathrm{in})}(\mathbf{r}_1,\omega)S^{(\mathrm{in})}(\mathbf{r}_2,\omega)]^{1/2}}, \tag{2}$$

where the incident *spectral density* is defined as

$$S^{(\mathrm{in})}(\mathbf{r},\omega) \equiv W^{(\mathrm{in})}(\mathbf{r},\mathbf{r},\omega). \tag{3}$$

We consider a general, three-dimensional crystalline array of identical point scatterers. In that case the *scattering potential* $F(\mathbf{r},\omega)$ can be written as

$$F(\mathbf{r},\omega) = F_0(\omega)\sum_{\mathbf{R}}\delta^3(\mathbf{r}-\mathbf{R}), \tag{4}$$

with $F_0(\omega)\in\mathbb{R}$, δ^3 denoting the three-dimensional Dirac δ function, and with the position vectors of the scatterers given by

$$\mathbf{R} = N_1\mathbf{a}_1 + N_2\mathbf{a}_2 + N_3\mathbf{a}_3. \tag{5}$$

Here $\mathbf{a}_1$, $\mathbf{a}_2$, and $\mathbf{a}_3$ denote the *direct lattice vectors* that span the crystal, with N_i any integer, and $i = 1, 2, 3$. The periodicity of $F(\mathbf{r},\omega)$ allows us to express it as a Fourier series, i.e.,

$$F(\mathbf{r},\omega) = \sum_{\mathbf{G}} f(\mathbf{G},\omega)\, e^{i\mathbf{G}\cdot\mathbf{r}}, \tag{6}$$

with $f(\mathbf{G},\omega)$ the *structure factor* and $\mathbf{G}$ a *reciprocal lattice vector* [16]. The structure factor is given by the expression

$$f(\mathbf{G},\omega) = V^{-1}\int_V F(\mathbf{r},\omega)\, e^{-i\mathbf{G}\cdot\mathbf{r}}\, d^3r, \tag{7}$$

where V denotes the volume of a unit cell, over which the integration extends. From this it follows that in our case

$$f(\mathbf{G},\omega) = F_0(\omega), \tag{8}$$

for all vectors $\mathbf{G}$.

Within the validity of the first-order Born approximation [18], the scattered field in a direction indicated by the unit vector $\mathbf{s} = (s_x, s_y, s_z)$, is given by the formula

$$U^{(\mathrm{sca})}(r\mathbf{s},\omega) = \int_{\mathbb{R}^3} U^{(\mathrm{in})}(\mathbf{r}',\omega)G(r\mathbf{s},\mathbf{r}',\omega)F(\mathbf{r}',\omega)\, d^3r', \tag{9}$$

where $\mathbf{r} = r\mathbf{s}$ is a point of observation, and $G(r\mathbf{s},\mathbf{r}',\omega)$ is the outgoing free-space Green's function pertaining to the Helmholtz equation. Because the scattering potential is identically zero outside the domain of the scatterer, we have extended the integration in Eq. (9) to the entire three-dimensional space, i.e., to $\mathbb{R}^3$. Far away from the scatterer the Green's function takes on the asymptotic form

$$G(r\mathbf{s},\mathbf{r}',\omega) = \frac{e^{ik|\mathbf{r}-\mathbf{r}'|}}{|\mathbf{r}-\mathbf{r}'|} \sim \frac{e^{ikr}}{r}\, e^{-ik\mathbf{s}\cdot\mathbf{r}'}, \tag{10}$$

where k denotes the wavenumber associated with frequency ω. The spectral density of the scattered field is, in strict analogy with Eq. (3), given by the expression

$$S^{(\mathrm{sca})}(r\mathbf{s},\omega) = \langle U^{(\mathrm{sca})*}(r\mathbf{s},\omega)U^{(\mathrm{sca})}(r\mathbf{s},\omega)\rangle. \tag{11}$$

On substituting from Eqs. (6), (8), (9), and (10) into Eq. (11), and interchanging the order of ensemble averaging and integration, we obtain

$$S^{(\mathrm{sca})}(r\mathbf{s},\omega) = \frac{F_0^2(\omega)}{r^2}\int_{\mathbb{R}^6} W^{(\mathrm{in})}(\mathbf{r}',\mathbf{r}'',\omega)e^{-ik\mathbf{s}\cdot(\mathbf{r}''-\mathbf{r}')} \times \sum_{\mathbf{G}} e^{-i\mathbf{G}\cdot\mathbf{r}'}\sum_{\mathbf{H}} e^{i\mathbf{H}\cdot\mathbf{r}''}\, d^3r'd^3r'', \tag{12}$$

with the cross-spectral density function $W^{(\mathrm{in})}(\mathbf{r}',\mathbf{r}'',\omega)$ of the incident field given by Eq. (1), and $\mathbf{G}$ and $\mathbf{H}$ denoting a reciprocal lattice vector. Interchanging integration and summation, and rearranging terms yields

$$S^{(\mathrm{sca})}(r\mathbf{s},\omega) = \frac{F_0^2(\omega)}{r^2}\sum_{\mathbf{G}}\sum_{\mathbf{H}}\int_{\mathbb{R}^6} W^{(\mathrm{in})}(\mathbf{r}',\mathbf{r}'',\omega) \times e^{i\mathbf{r}'\cdot(k\mathbf{s}-\mathbf{G})}e^{i\mathbf{r}''\cdot(\mathbf{H}-k\mathbf{s})}\, d^3r'd^3r''. \tag{13}$$

We note that this expression relates the scattered field to the six-dimensional spatial Fourier transform of the cross-spectral density of the incident field. To simplify the notation we omit the ω-dependence from now on.

Next we make use of the fact that, far away from the source, the cross-spectral density function itself is also a Fourier transform, namely

$$W^{(\mathrm{in})}(\mathbf{r}',\mathbf{r}'') = \left(\frac{k}{2\pi\Delta z}\right)^2 e^{ik(z''-z')}\iint_{z=0} W^{(0)}(\boldsymbol{\rho}_1,\boldsymbol{\rho}_2) \times e^{-ik(\boldsymbol{\rho}''\cdot\boldsymbol{\rho}_2-\boldsymbol{\rho}'\cdot\boldsymbol{\rho}_1)/\Delta z}\, d^2\rho_1 d^2\rho_2, \tag{14}$$

where the superscript (0) indicates the source plane $z = 0$, and with $\mathbf{r}' = (\boldsymbol{\rho}', z')$ and $\mathbf{r}'' = (\boldsymbol{\rho}'', z'')$. The distance Δz between the source and the scatterer is illustrated in Fig. 1. Equation (14) is derived in the Appendix. On making use of this expression

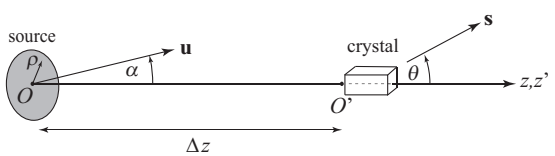

FIG. 1. Illustrating the notation. The origin O of the first coordinate system is taken in the source plane $z = 0$. The origin O' of the primed coordinates is taken at $(x, y, z) = (0, 0, \Delta z)$.

in Eq. (13) we get the formula

$$S^{(\mathrm{sca})}(r\mathbf{s}) = \left(\frac{F_0 k}{2\pi r \Delta z}\right)^2 \sum_{\mathbf{G}} \sum_{\mathbf{H}} \int_{\mathbb{R}^6} \iint_{z=0} e^{ik(z''-z')} W^{(0)}(\boldsymbol{\rho}_1, \boldsymbol{\rho}_2) e^{-ik(\boldsymbol{\rho}''\cdot\boldsymbol{\rho}_2 - \boldsymbol{\rho}'\cdot\boldsymbol{\rho}_1)/\Delta z} e^{i\mathbf{r}'\cdot(k\mathbf{s}-\mathbf{G})} e^{i\mathbf{r}''\cdot(\mathbf{H}-k\mathbf{s})}\, d^2\rho_1 d^2\rho_2 d^3r' d^3r''. \quad (15)$$

Writing this out in Cartesian components gives

$$S^{(\mathrm{sca})}(r\mathbf{s}) = \left(\frac{F_0 k}{2\pi r \Delta z}\right)^2 \sum_{\mathbf{G}} \sum_{\mathbf{H}} \int_{\mathbb{R}} e^{-ikz'} e^{iz'(ks_z - G_z)}\, dz' \int_{\mathbb{R}} e^{ikz''} e^{iz''(H_z - ks_z)}\, dz'' \int_{\mathbb{R}^8} W^{(0)}(x_1, y_1, x_2, y_2)$$
$$\times\ e^{-ik(x''x_2 + y''y_2 - x'x_1 - y'y_1)/\Delta z} e^{ix'(ks_x - G_x)} e^{iy'(ks_y - G_y)} e^{ix''(H_x - ks_x)} e^{iy''(H_y - ks_y)}\, dx_1 dy_1 dx_2 dy_2 dx' dy' dx'' dy''. \quad (16)$$

The integrals over z' and z'' are readily evaluated to give

$$\int_{\mathbb{R}} e^{iz'(ks_z - G_z - k)}\, dz' = 2\pi\delta(ks_z - G_z - k), \quad (17)$$

and

$$\int_{\mathbb{R}} e^{iz''(H_z - ks_z + k)}\, dz'' = 2\pi\delta(H_z - ks_z + k), \quad (18)$$

respectively. In order to have a scattered field that is nonzero, Eqs. (17) and (18) have to be satisfied simultaneously. This implies that

$$G_z = H_z = k(s_z - 1). \quad (19)$$

Similarly, the integrals over the remaining four primed variables also yield δ-functions, for example,

$$\int_{\mathbb{R}} e^{ix'(kx_1/\Delta z + ks_x - G_x)}\, dx' = 2\pi\delta(kx_1/\Delta z + ks_x - G_x). \quad (20)$$

Thus, we find the four relations

$$x_1 = \Delta z(G_x/k - s_x), \quad (21)$$

$$y_1 = \Delta z(G_y/k - s_y), \quad (22)$$

$$x_2 = \Delta z(H_x/k - s_x), \quad (23)$$

$$y_2 = \Delta z(H_y/k - s_y). \quad (24)$$

Substitution in Eq. (16) gives the final result

$$S^{(\mathrm{sca})}(r\mathbf{s}) = \left(\frac{F_0 4\pi^2 \Delta z}{kr}\right)^2 \sum_{\mathbf{G},\mathbf{H}} W^{(0)}(x_1, y_1, x_2, y_2), \quad (25)$$

with the arguments (x_1, y_1, x_2, y_2) of the cross-spectral density function $W^{(0)}$ given by Eqs. (21)–(24), and the double summation over the reciprocal lattice vectors such that $G_z = H_z$. Equation (25) is a general expression for the far-zone scattered field in terms of the cross-spectral density function of the source and the reciprocal lattice of the crystal.

III. ORTHORHOMBIC CRYSTALS

From here on we assume the scattering structure to be an orthorhombic crystal [16], consisting of unit cells with sides a, b, c, as sketched in Fig. 2. We note that this choice of coordinate axes means that we consider a field that is normally incident along the z direction.

For an orthorhombic crystal the Cartesian components of its reciprocal lattice vectors are given by the formulas

$$G_x = 2\pi\frac{n_1}{a}, \quad (26)$$

$$G_y = 2\pi\frac{n_2}{b}, \quad (27)$$

$$G_z = 2\pi\frac{n_3}{c}, \quad (28)$$

and

$$H_x = 2\pi\frac{m_1}{a}, \quad (29)$$

$$H_y = 2\pi\frac{m_2}{b}, \quad (30)$$

$$H_z = 2\pi\frac{m_3}{c}, \quad (31)$$

with the indices n_i and m_i any integer, and $i = 1, 2, 3$. Equation (19) yields the restriction $n_3 = m_3$. The above expressions will be used in Eqs. (21)–(24).

IV. GAUSSIAN SCHELL-MODEL SOURCES

For a planar source of the Gaussian Schell model type [17], the cross-spectral density function in the source plane reads

$$W^{(0)}(\boldsymbol{\rho}_1, \boldsymbol{\rho}_2) = \sqrt{S^{(0)}(\boldsymbol{\rho}_1) S^{(0)}(\boldsymbol{\rho}_2)}\, \mu^{(0)}(\boldsymbol{\rho}_2 - \boldsymbol{\rho}_1), \quad (32)$$

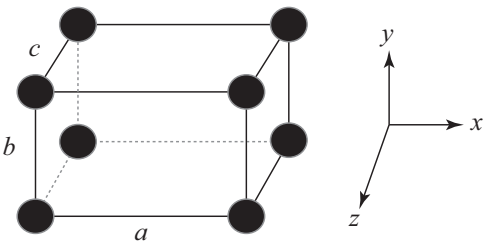

FIG. 2. A rectangular parallelepiped unit cell of eight identical point scatterers. The direct lattice vectors are $\mathbf{a}_1 = a\hat{\mathbf{x}}, \mathbf{a}_2 = b\hat{\mathbf{y}}$ and $\mathbf{a}_3 = c\hat{\mathbf{z}}$. The orthorhombic scatterer is assumed to consist of many of these unit cells.

with the spectral density and the spectral degree of coherence both having a Gaussian form, i.e.,

$$S^{(0)}(\boldsymbol{\rho}) = A^2 e^{-\rho^2/2\sigma_S^2}, \tag{33}$$

$$\mu^{(0)}(\boldsymbol{\rho}_2 - \boldsymbol{\rho}_1) = e^{-(\boldsymbol{\rho}_2-\boldsymbol{\rho}_1)^2/2\sigma_\mu^2}. \tag{34}$$

Here A^2 denotes the maximum spectral density, σ_S the effective source width, and σ_μ the effective transverse coherence length.

Let us next make the additional assumption that the source is quasihomogeneous. For such sources the spectral density $S^{(0)}(\boldsymbol{\rho})$ changes much more slowly with $\boldsymbol{\rho}$ than the spectral degree of coherence $\mu^{(0)}(\boldsymbol{\rho}_2 - \boldsymbol{\rho}_1)$ changes with $|\boldsymbol{\rho}_2 - \boldsymbol{\rho}_1|$. That implies that $\sigma_\mu^2 \ll \sigma_S^2$. The far-zone spectral degree of coherence of the field that is generated by such a source satisfies the reciprocity relation [17, Sec. 5.3.2],

$$\mu^{(\infty)}(r_1\mathbf{s}_1, r_2\mathbf{s}_2) = \frac{\tilde{S}^{(0)}[k(\mathbf{s}_{2\perp} - \mathbf{s}_{1\perp})]}{\tilde{S}^{(0)}(0)} e^{ik(r_2-r_1)}, \tag{35}$$

where the superscript (∞) indicates points in the far zone, and $\mathbf{s}_{i\perp} = (s_{ix}, s_{iy})$, with $i = 1, 2$, are the transverse parts of the directional unit vector $\mathbf{s}_i$. If we apply the spectral density distribution Eq. (33) to this expression, we find for the spectral degree of coherence of the field that is incident on the crystal the equation

$$\mu^{(\mathrm{in})}(r_1\mathbf{s}_1, r_2\mathbf{s}_2) = e^{-k^2\sigma_S^2(\mathbf{s}_{2\perp}-\mathbf{s}_{1\perp})^2/2} e^{ik(r_2-r_1)}. \tag{36}$$

Equation (36) shows that we can change the state of coherence of the incident field, or more precisely, its effective transverse coherence length, by changing the width σ_S of the source.

If we substitute from Eq. (32) into Eq. (25) for the case of an orthorhombic crystal, as was described in the previous section, we obtain the formula

$$S^{(\mathrm{sca})}(r\mathbf{s}) = \beta \sum_{\substack{n_i, m_j \\ n_3 = m_3}} \exp\left\{ -\frac{(\Delta z)^2}{4\sigma_S^2}\left[\left(\frac{2\pi n_1}{ka} - s_x\right)^2 + \left(\frac{2\pi n_2}{kb} - s_y\right)^2 + \left(\frac{2\pi m_1}{ka} - s_x\right)^2 + \left(\frac{2\pi m_2}{kb} - s_y\right)^2\right]\right\}$$
$$\times \exp\left(-\frac{(\Delta z)^2}{2\sigma_\mu^2}\left\{\left[\frac{2\pi}{ka}(m_1 - n_1)\right]^2 + \left[\frac{2\pi}{kb}(m_2 - n_2)\right]^2\right\}\right), \tag{37}$$

with $i, j = 1, 2, 3$, and where for brevity we have introduced the parameter β, where

$$\beta = \left(\frac{A F_0 4\pi^2 \Delta z}{kr}\right)^2. \tag{38}$$

The maximum term in the summation occurs when the arguments of both exponentials are zero, i.e., when $m_1 = n_1$ and $m_2 = n_2$, and for a scattering direction $\mathbf{s}$ such that

$$s_x = \frac{\lambda n_1}{a}, \tag{39}$$

$$s_y = \frac{\lambda n_2}{b}, \tag{40}$$

with the wavelength $\lambda = 2\pi/k$. For the longitudinal component of $\mathbf{s}$ we have from Eqs. (19) and (28) that

$$s_z = 1 + \frac{\lambda n_3}{c}. \tag{41}$$

These three formulas are the well-known von Laue equations [3, Sec. 13.1.3]. They indicate the directions $\mathbf{s}$ of maximum scattering for an incident field that is spatially fully coherent.

On making use in Eq. (37) of the assumption that $\sigma_\mu^2 \ll \sigma_S^2$, it follows that we may safely neglect all terms for which $m_1 \neq n_1$ and $m_2 \neq n_2$. This then gives

$$S^{(\mathrm{sca})}(r\mathbf{s}) = \beta \sum_{n_i} \exp\left\{ -\frac{(\Delta z)^2}{2\sigma_S^2}\left[\left(\frac{2\pi n_1}{ka} - s_x\right)^2 + \left(\frac{2\pi n_2}{kb} - s_y\right)^2\right]\right\}. \tag{42}$$

Equation (42) describes the scattered field as a sum of terms. Each term is characterized by the integer triplet (n_1, n_2, n_3). The value of these integers determines a specific wavelength λ and a direction $\mathbf{s}$ at which the scattering reaches a maximum, a so-called von Laue spot. It is worth noting that Eq. (42) does *not* depend on the coherence length σ_μ of the source, however it *does* depend on the state of coherence of the incident field. This is because for a distant quasihomogeneous Gaussian Schell-model source, the reciprocity relation Eq. (36) implies that the coherence of the incident field is governed by the effective source size σ_S, rather than σ_μ. When this source size is decreased, the spectral degree of coherence of the field that is incident on the crystal, is increased.

We illustrate our results by considering the example of an orthorhombic crystal with unit cells with sides

$$a = 1.0 \times 10^{-9}\mathrm{m}, \tag{43}$$

$$b = 1.2 \times 10^{-9}\mathrm{m}, \tag{44}$$

$$c = 1.5 \times 10^{-9}\mathrm{m}. \tag{45}$$

We study a single scattering direction by choosing a triplet (n_1, n_2, n_3). The three von Laue equations, together with the requirement that $\mathbf{s}$ is a unit vector, i.e.,

$$s_x^2 + s_y^2 + s_z^2 = 1, \tag{46}$$

form an over-determined system that will only be satisfied for a specific wavelength. For example, for the

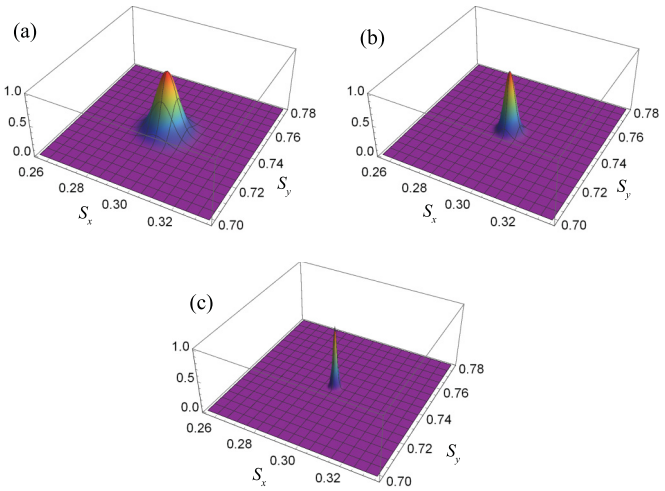

FIG. 3. Distribution of the normalized scattered intensity around the direction indicated by the von Laue equations for different values of the effective source width, and hence a different transverse coherence length of the incident field. (a) $\sigma_S = 5.0 \times 10^{-3}$ m; (b) $\sigma_S = 2.5 \times 10^{-3}$ m; (c): $\sigma_S = 1.0 \times 10^{-3}$ m. In these examples $n_1 = 1, n_2 = 3, n_3 = -2$, and $\Delta z = 1$ m.

choice

$$n_1 = 1, \tag{47}$$

$$n_2 = 3, \tag{48}$$

$$n_3 = -2, \tag{49}$$

it is found that $\lambda = 2.95 \times 10^{-10}$ m, and hence that $s_x = 0.29$, $s_y = 0.73$, and $s_z = 0.60$.

We note that, apart from this particular value of the wavelength, there exists, for every choice of (n_1, n_2, n_3), the trivial solution $\lambda = 0$, and hence $s_z = 1$. This corresponds to a forward-propagating field with an infinite frequency. Since this is nonphysical, we exclude this solution. We will return to the issue of spurious solutions in the next section.

The influence of the state of coherence of the incident field on the distribution of the scattered field around the direction specified by the von Laue equations is evaluated by calculating a single term of the summation in Eq. (42):

$$S^{(\mathrm{sca})}(n_1,n_2,n_3) = \beta \exp\left\{ -\frac{(\Delta z)^2}{2\sigma_S^2}\left[\left(\frac{2\pi n_1}{ka} - s_x\right)^2 + \left(\frac{2\pi n_2}{kb} - s_y\right)^2\right]\right\}, \tag{50}$$

where we have changed the arguments of $S^{(\mathrm{sca})}$ from $(r\mathbf{s})$ to the triplet (n_1, n_2, n_3).

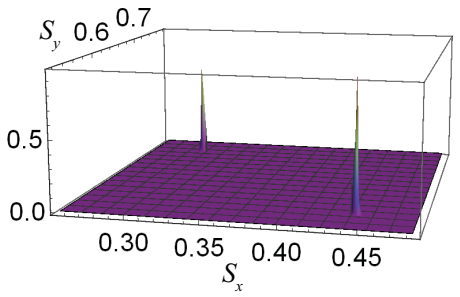

FIG. 4. Distribution of the normalized scattered intensity around two von Laue spots. The left-hand peak corresponds to $(n_1, n_2, n_3) = (1, 3, -2)$ and hence $\lambda = 2.95 \times 10^{-10}$ m. The right-hand peak is for $(n_1, n_2, n_3) = (2, 3, -2)$, and thus $\lambda = 2.21 \times 10^{-10}$ m. In these two examples $\sigma_S = 1.0 \times 10^{-3}$ m and $\Delta z = 1$ m.

An example is presented in Fig. 3. The source width σ_S decreases in going from Fig. 3(a) to 3(c). This means that the spectral degree of coherence of the incident field increases. It is seen that the circular, Gaussian intensity distribution, which is centered around the von Laue direction, gets narrower when the spatial coherence of the incident field increases and becomes more and more point-like.

Let us next choose a second scattering direction by setting

$$n_1 = 2, \tag{51}$$

$$n_2 = 3, \tag{52}$$

$$n_3 = -2. \tag{53}$$

We now find that $\lambda = 2.21 \times 10^{-10}$ m, and hence that $s_x = 0.44$, $s_y = 0.55$, and $s_z = 0.70$. It is clear from Fig. 4 that these two diffraction peaks are well separated, both directionally and spectrally.

V. UNCORRELATED, INFINITELY THIN ANNULAR SOURCES

We next consider the idealized case of a completely incoherent, infinitely thin "δ-ring" source. If this ring has a uniform spectral density A^2, and is of radius R, then the cross-spectral density of the field in the source plane is given by the expression

$$W^{(0)}(\boldsymbol{\rho}_1,\boldsymbol{\rho}_2) = A^2\delta(\rho_1 - R)\delta^2(\boldsymbol{\rho}_2 - \boldsymbol{\rho}_1), \tag{54}$$

where δ and δ^2 represent the one- and two-dimensional Dirac δ function, respectively. Such a source produces a J_0 Bessel-correlated field in its far zone. The approximate experimental realization of such a field was reported in Ref. [19].

If we substitute from Eq. (54) into Eq. (25) for the case of an orthorhombic crystal as described in Sec. III, we get the expression

$$S^{(\mathrm{sca})}(r\mathbf{s}) = \beta \sum_{\substack{n_i,m_j \\ n_3=m_3}} \delta\left\{\Delta z\left[\left(\frac{2\pi n_1}{ka} - s_x\right)^2 + \left(\frac{2\pi n_2}{kb} - s_y\right)^2\right]^{1/2} - R\right\}\delta\left[\frac{2\pi}{ka}(n_1 - m_1)\right]\delta\left[\frac{2\pi}{kb}(n_2 - m_2)\right], \tag{55}$$

$$= \beta \sum_{n_i} \delta\left\{\Delta z\left[\left(\frac{2\pi n_1}{ka} - s_x\right)^2 + \left(\frac{2\pi n_2}{kb} - s_y\right)^2\right]^{1/2} - R\right\}. \tag{56}$$

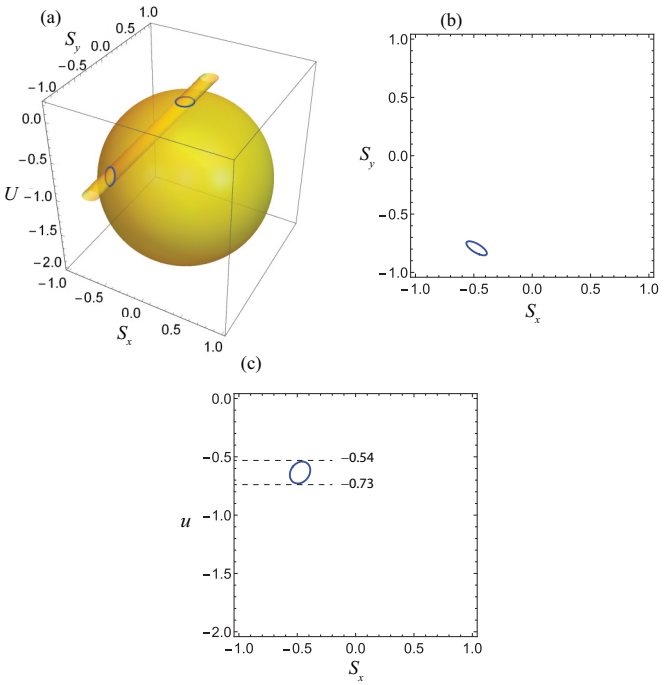

FIG. 5. (a) An oblique, elliptic cylinder and a unit sphere in (s_x, s_y, u)-space. The sphere is centered on $(0, 0, -1)$, and the cylinder has a radius $R/\Delta z$ in the horizontal plane. The intersections of the cylinder and the sphere are indicated by the two blue curves. (b) The projection of the lower intersection onto the s_x, s_y plane. (c) The projection of the lower intersection onto the s_x, u plane. In these examples $a = 1 \times 10^{-9}$ m, $b = 1.2 \times 10^{-9}$ m, $c = 1.5 \times 10^{-9}$ m, $n_1 = -1$, $n_2 = -2$, $n_3 = -2$, $R = 0.1$ m, and $\Delta z = 1$ m.

In order to determine the components of the directional vector $\mathbf{s}$ and the wavelength λ, we recall Eq. (41),

$$s_z = 1 + u, \tag{57}$$

where we defined the scaled wavelength u as

$$u \equiv \frac{\lambda n_3}{c}. \tag{58}$$

The first requirement, that $|\mathbf{s}| = 1$, defines a unit sphere in (s_x, s_y, u)-space that is centered around the point $(0, 0, -1)$, as is shown in Fig. 5. The second condition, which is derived from Eqs. (56) and (58), reads

$$\left(u\frac{cn_1}{n_3 a} - s_x\right)^2 + \left(u\frac{cn_2}{n_3 b} - s_y\right)^2 = \frac{R^2}{(\Delta z)^2}. \tag{59}$$

This defines an oblique, elliptic cylinder, whose intersection with any horizontal plane $u =$ constant, is a circle with center $(s_x, s_y) = (ucn_1/n_3 a, ucn_2/n_3 b)$, and with radius $R/\Delta z$. From this expression it follows readily that the central axis of the cylinder is the line given by the formula

$$(s_x, s_y, u) = (ucn_1/n_3 a, ucn_2/n_3 b, u). \tag{60}$$

For any choice of the triplet (n_1, n_2, n_3), the directions of nonzero scattering and the wavelength are given by the intersections of the cylinder and the unit sphere. These will be two closed curves, as indicated in blue in the example shown in Fig. 5(a). The upper curve, near $u = 0$, is the partially coherent analog of the spurious solution that we discussed below Eq. (49), and we will therefore not consider it.

The assumption that the scatterer is in the far zone of the source means that R is much smaller than Δz. This implies that the cylinder is quite narrow. According to Eq. (57), an intersection of the cylinder in the upper half of the sphere ($u > -1$), corresponds to forward scattering ($s_z > 0$), whereas an intersection in the lower portion of the sphere represents backscattering ($s_z < 0$). Instead of a single von Laue direction, we now have a range of scattering directions, each represented by a point on the intersectional curve. Since these points each have a distinct u coordinate, Eq. (58) implies that they all represent scattering at a distinct wavelength, i.e., the von Laue curves show dispersion. It is worth remarking that this spread in u values, and hence the dispersion, will be more pronounced for oblique scattering than for scattering in the forward direction.

The projection of the sphere-cylinder intersection onto the the s_x, s_y plane is obtained by substituting $u = -1 \pm (1 - s_x^2 - s_y^2)^{1/2}$ into Eq. (59), with the plus (minus) sign taken for intersections in the upper (lower) half of the sphere. This gives the formula

$$\frac{R^2}{(\Delta z)^2} = \left[\left(-1 \pm \sqrt{1 - s_x^2 - s_y^2}\right)\frac{cn_1}{n_3 a} - s_x\right]^2 + \left[\left(-1 \pm \sqrt{1 - s_x^2 - s_y^2}\right)\frac{cn_2}{n_3 b} - s_y\right]^2. \tag{61}$$

The projection of the lower curve of Fig. 5(a) is plotted in Fig. 5(b). This curve represents scattering along a range of directions $\mathbf{s}$, each with a specific value of u, and hence with a different wavelength. The variation of the wavelength with the direction $\mathbf{s}$ can be studied by projecting the intersection onto the s_x, u plane. This is done by substituting $s_y = \pm[1 - s_x^2 - (1 + u)^2]^{1/2}$ into Eq. (59), with the plus (minus) sign taken when s_y is positive (negative). The result is

$$\frac{R^2}{(\Delta z)^2} = \left[u\frac{cn_1}{n_3 a} - s_x\right]^2 + \left[u\frac{cn_2}{n_3 b} \mp \sqrt{1 - s_x^2 - (1 + u)^2}\right]^2. \tag{62}$$

The projection of the lower curve is shown in Fig. 5(c). It is seen that the value of u varies between -0.54 and -0.73. According to Eq. (58), this corresponds to a wavelength range of $4.05 \times 10^{-10}\,\text{m} \leqslant \lambda \leqslant 5.47 \times 10^{-10}\,\text{m}$.

The distinction between forward and backward scattering can be made by considering the angle, γ say, between the axis of the cylinder and the positive u axis. It follows from Eq. (60) that

$$\tan\gamma = \sqrt{\left(\frac{cn_1}{n_3 a}\right)^2 + \left(\frac{cn_2}{n_3 b}\right)^2}. \tag{63}$$

Ignoring the finite radius of the cylinder for simplicity, the lowest intersection of the cylinder with the sphere will be above the equator ($u = -1$) when this angle exceeds 45°. Hence, we conclude that forward scattering occurs when

$$\left(\frac{cn_1}{n_3 a}\right)^2 + \left(\frac{cn_2}{n_3 b}\right)^2 > 1. \tag{64}$$

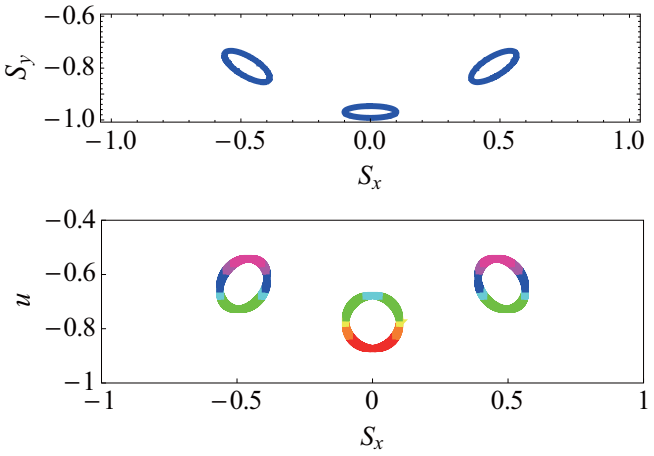

FIG. 6. (a) Three different von Laue patterns scattered in the forward direction ($s_z > 0$) for, from left to right, $n_1 = -1, 0, 1$, and $n_2 = n_3 = -2$. (b) The projection of these curves onto the s_x, u plane, showing their colors in the visible spectrum. In this example, $a = 1 \times 10^{-6}$ m, $b = 1.2 \times 10^{-6}$ m, $c = 1.5 \times 10^{-6}$ m, $R = 0.1$ m, and $z = 1$ m.

When this quantity is less than unity, the scattering is in the backward direction.

Colorful von Laue patterns in the visible spectrum can be produced by crystals with sides on the order of microns. Examples of three symmetrically located, forward-scattered patterns ($s_z > 0$), are plotted in Fig. 6(a). Their projection onto the s_x, u plane is shown in Fig. 6(b). Using Eq. (58), it is found that the wavelengths for these three ellipses range from 405 to 660 nm, as is indicated in the color rendering. By increasing the distance Δz between the source and the crystal (see Fig. 1), one gradually approaches the case of spatially coherent illumination. This should lead to a decrease in dispersion. Indeed it found for example, that when Δz is increased from 1 to 5 m, the wavelength range is reduced to 465 to 600 nm.

Examples of scattering in the backward direction ($s_z < 0$) are presented in Fig. 7. Near-circular, overlapping intensity patterns are produced with a wavelength interval from 444 to 480 nm. The directional radius of these patterns, i.e., their spread in the s_x,s_y plane, can easily be tailored by changing either the source radius R or the source-crystal distance Δz. Decreasing the ratio $R/\Delta z$ decreases the directional radius.

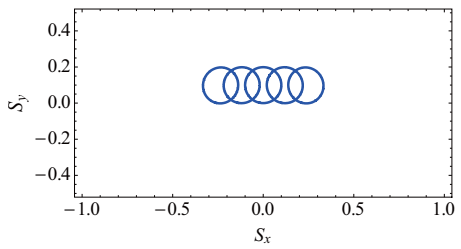

FIG. 7. Showing five different backscattered von Laue rings for, from left to right, $n_1 = -2, -1, 0, 1, 2$, and $n_2 = 1$ and $n_3 = -25$. In this example $a = 4 \times 10^{-6}$ m, $b = 4.8 \times 10^{-6}$ m, $c = 6.0 \times 10^{-6}$ m, $R = 0.1$ m, and $\Delta z = 1$ m.

VI. CONCLUSIONS

We have analyzed the role of spatial coherence in scattering from a periodic potential. This was done within the context of the so-called von Laue method, in which a polychromatic field is diffracted by a crystal with a fixed orientation. A general expression, Eq. (25), that relates the scattered field to the cross-spectral density of the source, was derived. This result was applied to two different types of partially coherent sources. Quasihomogeneous Gaussian Schell model sources (GSM) and δ-correlated, thin annular sources. The sphere-cylinder construction that we used for the latter type can, at least in principle, also be applied to the GSM source. However, we chose, for that case at least, to stay closer to the traditional treatment. The GSM sources were seen to produce von Laue spots whose size is directly related to the size of the source. The annular sources were found to generate elliptical von Laue patterns rather than spots. Both the dispersion and the angular spread of these patterns can be tuned by changing the source radius or the distance between the source and the crystal. In summary, we have shown how spatial coherence can be used to tailor scattering by an object with a periodic potential. Our work may be extended to sources with different shapes and correlation functions, other crystals, and crystals with a different orientation.

ACKNOWLEDGMENTS

This material is based upon work supported by the Air Force Office of Scientific Research under Award No. FA9550-16-1-0119, the Natural Science Basic Research Plan in Shaanxi Province of China (Grant No. 2016JQ1011), and the National Natural Science Foundations of China (NSFC) (Grant No. 11504296).

APPENDIX: DERIVATION OF EQUATION (14)

Consider a secondary, partially coherent, planar source that is situated in the plane $z = 0$, as sketched in Fig. 1. The symbol $\boldsymbol{\rho} = (x, y)$ denotes a transverse vector. The coherence properties of the source field at two points $\boldsymbol{\rho}_1$ and $\boldsymbol{\rho}_2$ are characterized by the cross-spectral density function,

$$W^{(0)}(\boldsymbol{\rho}_1, \boldsymbol{\rho}_2) = \langle U^{(0)*}(\boldsymbol{\rho}_1) U^{(0)}(\boldsymbol{\rho}_2) \rangle, \tag{A1}$$

where the superscript (0) indicates the source plane. If the scatterer is located far away from the source, then the incident cross-spectral density of the incident field equals [17, Eq. 5.3-4]

$$\begin{aligned} W^{(\mathrm{in})}&(r_1\mathbf{u}_1, r_2\mathbf{u}_2) \\ &= \left(\frac{k}{2\pi}\right)^2 \frac{\exp[ik(r_2 - r_1)]}{r_1 r_2} \cos\alpha_1 \cos\alpha_2 \\ &\quad \times \iint_{z=0} W^{(0)}(\boldsymbol{\rho}_1, \boldsymbol{\rho}_2) \\ &\quad \times \exp[-ik(\mathbf{u}_{2\perp} \cdot \boldsymbol{\rho}_2 - \mathbf{u}_{1\perp} \cdot \boldsymbol{\rho}_1)]\, d^2\rho_1 d^2\rho_2, \end{aligned} \tag{A2}$$

where $\mathbf{u}_{1\perp}$ and $\mathbf{u}_{2\perp}$ are the transverse parts of the directional unit vectors $\mathbf{u}_1$ and $\mathbf{u}_2$. These two vectors are under an angle α_1 and α_2, respectively, with the positive z axis. The scatterer is a distance Δz from the source. Because the linear dimensions of the scatterer may be assumed to be much smaller than Δz, the angles α_1 and α_2 are both small and hence $\cos\alpha_1 \approx \cos\alpha_2 \approx 1$. Furthermore, the factor $k(r_2 - r_1)$ where $r_i = |(\boldsymbol{\rho}_i, z_i)|$, with $i = 1$ or 2, can then be expressed as

$$k(r_2 - r_1) \approx k\big[z_2\big(1 + \rho_2^2/2z_2^2\big) - z_1\big(1 + \rho_1^2/2z_1^2\big)\big], \tag{A3}$$

$$\approx k(z_2 - z_1), \tag{A4}$$

where we have used the fact that ρ_1 and ρ_2 are both bounded by the transverse size of the scatterer. In addition, the finite size of the scatterer implies that the factor $1/r_1 r_2$ does not vary appreciably over its domain, i.e.,

$$\frac{1}{r_1 r_2} \approx \frac{1}{(\Delta z)^2}. \tag{A5}$$

On making use of these approximations in Eq. (A2) we obtain the expression

$$W^{(\mathrm{in})}(r_1\mathbf{u}_1, r_2\mathbf{u}_2) = \left(\frac{k}{2\pi\,\Delta z}\right)^2 \exp[ik(z_2 - z_1)] \iint_{z=0} W^{(0)}(\boldsymbol{\rho}_1, \boldsymbol{\rho}_2) \exp[-ik(\mathbf{u}_{2\perp}\cdot\boldsymbol{\rho}_2 - \mathbf{u}_{1\perp}\cdot\boldsymbol{\rho}_1)]\, d^2\rho_1 d^2\rho_2. \tag{A6}$$

Finally, Eq. (A6) must be expressed in terms of the primed variables defined in Fig. 1. This is done by noting that

$$z_2 - z_1 = z'' - z', \tag{A7}$$

$$\mathbf{u}_{1\perp} \approx \boldsymbol{\rho}'/\Delta z, \tag{A8}$$

$$\mathbf{u}_{2\perp} \approx \boldsymbol{\rho}''/\Delta z, \tag{A9}$$

and hence we obtain

$$W^{(\mathrm{in})}(\mathbf{r}', \mathbf{r}'') = \left(\frac{k}{2\pi\,\Delta z}\right)^2 \exp[ik(z'' - z')] \iint_{z=0} W^{(0)}(\boldsymbol{\rho}_1, \boldsymbol{\rho}_2) \exp[-ik(\boldsymbol{\rho}''\cdot\boldsymbol{\rho}_2 - \boldsymbol{\rho}'\cdot\boldsymbol{\rho}_1)/\Delta z]\, d^2\rho_1 d^2\rho_2, \tag{A10}$$

which is Eq. (14).

[1] R. W. James, *X-Ray Crystallography*, 4th ed. (Methuen and Co., London, 1950).

[2] N. W. Ashcroft and N. D. Mermin, *Solid State Physics* (Harcourt, Orlando, 1976).

[3] M. Born and E. Wolf, *Principles of Optics*, 7th (expanded) ed. (Cambridge University Press, Cambridge, 1999).

[4] J. Jannson, T. Jannson, and E. Wolf, Spatial coherence discrimination in scattering, Opt. Lett. **13**, 1060 (1988).

[5] F. Gori, C. Palma, and M. Santarsiero, A scattering experiment with partially coherent light, Opt. Commun. **74**, 353 (1990).

[6] J. J. Greffet, M. De La Cruz-Gutierrez, P. V. Ignatovich, and A. Radunsky, Influence of spatial coherence on scattering by a particle, J. Opt. Soc. Am. A **20**, 2315 (2003).

[7] J. Lindberg, T. Setälä, M. Kaivola, and A. T. Friberg, Spatial coherence effects in light scattering from metallic nanocylinders, J. Opt. Soc. Am. A **23**, 1349 (2006).

[8] T. van Dijk, D. G. Fischer, T. D. Visser, and E. Wolf, The Effects of Spatial Coherence on the Angular Distribution of Radiant Intensity Generated by Scattering on a Sphere, Phys. Rev. Lett. **104**, 173902 (2010).

[9] D. G. Fischer, T. van Dijk, T. D. Visser, and E. Wolf, Coherence effects in Mie scattering, J. Opt. Soc. Am. A **29**, 78 (2012).

[10] Y. Wang, S. Yan, D. Kuebel, and T. D. Visser, Dynamic control of light scattering using spatial coherence, Phys. Rev. A **92**, 013806 (2015).

[11] Y. Wang, H. F. Schouten, and T. D. Visser, Tunable, anomalous Mie scattering using spatial coherence, Opt. Lett. **40**, 4779 (2015).

[12] M. W. Hyde IV, Physical optics solution for the scattering of a partially coherent wave from a circular cylinder, Opt. Commun. **338**, 233 (2015).

[13] M. Dušek, Diffraction of partially coherent beams on three-dimensional periodic structures and the angular shifts of the diffraction maxima, Phys. Rev. E **52**, 6833 (1995).

[14] B. J. Hoenders and M. Bertolotti, Theory of partial coherence for weakly periodic media, J. Opt. Soc. Am. A **22**, 2682 (2005).

[15] E. Wolf, Diffraction of radiation of any state of spatial coherence on media with periodic structure, Opt. Lett. **38**, 4023 (2013).

[16] C. Kittel, *Introduction to Solid State Physics*, 6th ed. (Wiley, New York, 1986).

[17] L. Mandel and E. Wolf, *Optical Coherence and Quantum Optics* (Cambridge University Press, Cambridge, 1995).

[18] E. Wolf, *Introduction to the Theory of Coherence and Polarization of Light* (Cambridge University Press, Cambridge, 2007).

[19] S. B. Raghunathan, T. van Dijk, E. J. G. Peterman, and T. D. Visser, Experimental demonstration of an intensity minimum at the focus of a laser beam created by spatial coherence: Application to optical trapping of dielectric particles, Opt. Lett. **35**, 4166 (2010).